Automated grain size measurements from airborne remote sensing for long profile measurements of fluvial grain sizes

Patrice E. Carbonneau[1] and Normand Bergeron

Centre Eau, Terre et Environnement, Institut National de la Recherche Scientifique, Quebec, Quebec, Canada

Stuart N. Lane

Department of Geography, University of Durham, Durham, UK

Received 27 January 2005; revised 23 June 2005; accepted 9 August 2005; published 24 November 2005.

[1] Recent research has demonstrated that image processing can be applied to derive surficial median grain size data automatically from high-resolution airborne digital imagery in fluvial environments. However, at the present time, automated grain size measurement is limited to the dry exposed bed areas of the channel. This paper shows that the application area of automated grain size mapping can be extended in order to include the shallow wetted areas of the channel. The paper then proceeds to illustrate how automated grain size measurement in both dry and shallow wetted areas can be used to measure grain sizes automatically for long river lengths. For the present study, this results in a median grain size profile covering an 80 km long river which is constructed from over three million automated grain size measurements.

Citation: Carbonneau, P. E., N. Bergeron, and S. N. Lane (2005), Automated grain size measurements from airborne remote sensing for long profile measurements of fluvial grain sizes, *Water Resour. Res.*, *41*, W11426, doi:10.1029/2005WR003994.

1. Introduction

[2] System-scale data on surface grain size variability in gravel bed rivers are crucial for understanding and explaining sediment transfer processes [*Parker*, 1991; *Hoey and Ferguson*, 1994; *Seal and Paola*, 1995; *Seal et al.*, 1997; *Rice and Church*, 1996, 1998; *Rice*, 1999]. They are also linked to ecological processes including macroinvertebrates [*Rice et al.*, 2001a, 2001b] and the habitat preferences of fish such as salmonids [*Rimmer et al.*, 1983; *Cunjak*, 1988; *Heggenes*, 1996]. While it has been possible to quantify and to explain local gravel grain size variability for considerable time [*Bluck*, 1982; *Milne*, 1982] many of the pressing sedimentological [*Rice and Church*, 1996, 1998] and ecological [*Dunham and Rieman*, 1999; *Torgersen et al.*, 1999; *Thompson and Lee*, 2000] research questions are now emerging at the system scale, over many tens of kilometers rather than a few river reaches. The result is a need to scale upward [*Cunjak*, 1996; *Lewis et al.*, 1996; *Folt et al.*, 1998] without sacrificing the local spatial detail that is a crucial part of the sedimentological and ecological processes that in turn create larger scales of emergence. This requires analysis of the surface grain size of rivers as a continuously varying [*Fausch et al.*, 2002] patchy environment.

[3] The only technique that can feasibly deliver at scales ranging from the patch (meter scale) through to the drainage basin (kilometer scale) is remote sensing. Recent technological advances are changing the ways in which remote sensing can be applied to fluvial geomorphology as tasks which traditionally required labor intensive field work are now coming within the reach of remote sensing methods. Developments in digital image processing methods have already allowed for bathymetric measurements using airborne remote sensing [e.g., *Lyon et al.*, 1992; *Winterbottom and Gilvear*, 1997; *Roberts and Anderson*, 1999; *Westaway et al.*, 2003] and flow type classifications in relation to riverine habitat [*Marcus*, 2002; *Whited et al.*, 2002; *Marcus et al.*, 2003]. However, one of the remaining difficulties in the application of remote sensing to fluvial environments is that particle sizes, a fundamental descriptor of riverine habitats, cannot be easily measured with remote sensing methods.

[4] There is a significant body of literature describing how close range terrestrial remote sensing and image processing can be used to determine particle sizes automatically, both in a general civil engineering context [*Raschke and Hryciw*, 1997; *Ghalib and Hryciw*, 1999; *Shin and Hryciw*, 2004; *Wettimuny and Penumadu*, 2004] and a specific fluvial geomorphology context [*Adams*, 1979; *Ibbeken and Schleyer*, 1986; *Butler et al.*, 2001]. In such cases, the pixel resolution of the image is very small when compared to particle sizes. For example, *Raschke and Hryciw* [1997] used imagery where particle size as seen in the imagery, in pixel units, ranged from 50 to 2000 pixels. This implies that individual particle boundaries can be detected and therefore that individual particles can be measured. Unfortunately, these methods are not applicable to airborne and satellite imagery since the resulting ground resolution is too coarse to allow individual particles to be delineated. As an example, we shall considerer recent airborne sensors, such as the XEOS imaging system of

[1]Now at Department of Geography, University of Durham, Durham, UK.

0043-1397/05/2005WR003994$09.00

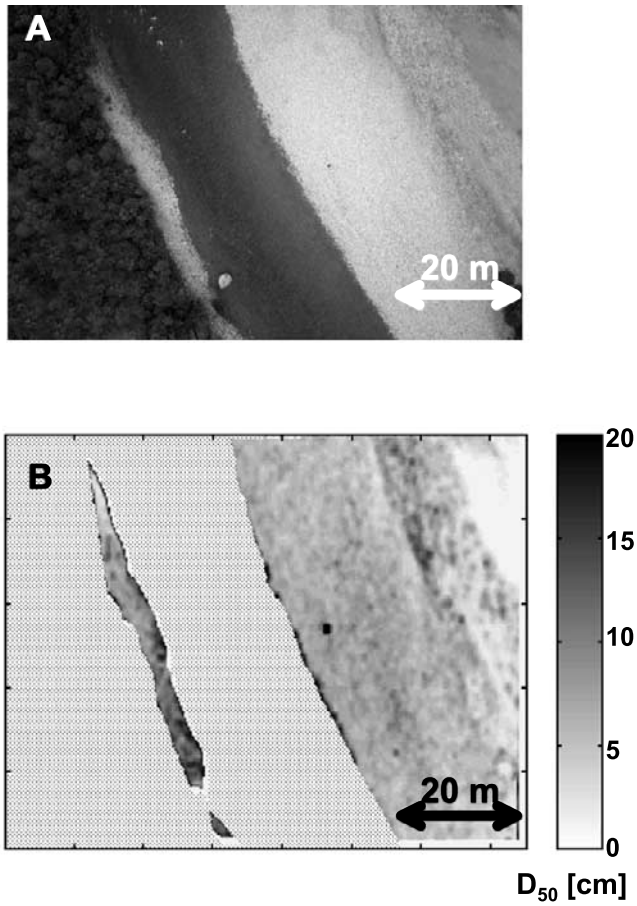

Figure 1. (a) Sample image from the Sainte-Marguerite River study site located at 48.38°N, 70.20°W. (b) Median grain size map for the dry exposed area in Figure 1a.

Génivar, Inc., or the ADS40 system of Leica, Inc., capable of maximum ground resolutions in the range of 3–5 cm. In fluvial terms, this would make sand and fine gravel sub pixel size and boulders, the largest clasts commonly of interest, up to 50 pixels in size. These equivalents are not sufficient to achieve individual particle delineation. Closer range studies could be used to generate high-resolution data, but this would be at the expense of having to become ground based, so undermining the need to generate system-scale data. However, *Carbonneau et al.* [2004] showed that automated grain size measurements of exposed reaches of a gravel bed river were possible from high-resolution airborne imagery. With rigorous testing, *Carbonneau et al.* [2004] demonstrated that local 2D semivariance maps derived from the imagery could be correlated to the median grain size in the image locality if all the relevant parameters are calibrated. These 2D semivariograms are calculated from a windowed application of local 2D semivariograms calculated from the image digital numbers (i.e., pixel brightness values) in the windowed area. Numerical testing by *Carbonneau et al.* [2004] established that the optimal window size for semivariance mapping is 33 × 33 pixel which, in the case of the 3 cm resolution imagery describes in this work, corresponds to a spatial area of 1 m^2. Each image is converted into a semivariance map by extracting the sill plane value for each local semivariogram and repeating this process until the entire image has been mapped. Each point in the semivariance map therefore gives a local semivariance value for a 1 m^2 area in the original image. An empirical relationship is then established between median grain sizes observed in the field and semivariance maps. For the image data set described by *Carbonneau et al.* [2004], the following calibration relationship was obtained:

$$D_{50} = 0.34\mathrm{SV} + 10.12, \quad (1)$$

where D_{50} is the median diameter of surface particles, in mm, in the 1 m^2 area and SV is the dimensionless local semivariance sill value in the corresponding 1 m^2 area of the image. While equation (1) gives the median grain size for a given 1 m^2 image patch as a function of local semivariance, initial results showed that local semivariance also correlates with other grain size fractions such as D_{16} and D_{84}, albeit with different regression relationships. Correlations with the 84th percentile were stronger. However, since the 50th percentile is a much more widely used parameter in geomorphology and fisheries habitat management, it was chosen as the principal objective.

[5] The empirical relationship (1) allows for an automated estimation of the grain sizes of the dry areas of the channel. Figure 1 shows a sample image with its associated grain size map. Closer examination of Figure 1b shows the sensitivity of the model. The sandy patch in the upper right corner of the image in Figure 1a is clearly detected as well as the coarser nature of the smaller bank on the left-hand side. Variations in grain size within the larger right bank are also well detected. The overall quality of these grain size estimates was validated with independent check data collected from sites scattered along a 10 km river reach and thus completely removed from the calibration data site. This allowed the precision of grain size estimates to be established as ±11 mm [*Carbonneau et al.*, 2004].

[6] Remotely generated, high-resolution and high-precision grain size estimates could be used to obtain grain size measurements over whole river basins and so allow investigation of large-scale grain size variations while simultaneously retaining the necessary local detail. However, the automated grain size measurement method presented by *Carbonneau et al.* [2004] is limited to dry exposed areas. Generally, such areas represent a small percentage of the total active river channel. For example, Table 1 shows the total surface areas for different channel subarea types measured on the whole length of the main channel of the Sainte-Marguerite River, Quebec, Canada. The channel has been divided into three classes: dry exposed bed; optically shallow wetted area, defined here as areas where the wetted bed is visible in the air photos; and deep wetted areas, defined here as areas where the

Table 1. Surface Area Coverages Associated With Each Channel Area Subtype for the Full 80 km Length of the Sainte-Marguerite River, Québec, Canada

Channel Subarea Type	Area, km^2	Percent of Total
Dry	0.6	19
Shallow water	2.4	67
Deep water	0.5	14
Total channel	3.5	100

wetted bed is not visible in the imagery. Since the dry area represents only 19% of the total channel area, dry area grain size mapping would provide an incomplete survey of grain sizes along this river and its usefulness for sedimentary link identification and other applications will be limited.

[7] The main goal of this paper is to develop the method described by *Carbonneau et al.* [2004] in order to allow for the automated estimation of median grain size in the wetted perimeter. Visual observations of the image data set used by *Carbonneau et al.* [2004] show that the river bed can be clearly seen in the shallow submerged areas which suggests that the method of *Carbonneau et al.* [2004] might be applied in this subarea, which represents 67% of the active channel area (Table 1). The secondary goal of this paper is to assess the usefulness of automated grain size mapping to the characterization of the long profile of grain size variations in the downstream direction and to determine if this method is capable of identifying the kinds of sedimentary link units now recognized to be a crucial component of both the sedimentology and the ecology of gravel bed rivers [e.g., *Rice and Church*, 1998; *Rice et al.*, 2001a].

2. Methods

2.1. Airborne Digital Imagery Acquisition

[8] The work discussed in this paper uses a set of high-resolution airborne imagery of the Sainte-Marguerite River in Quebec, Canada. The Sainte-Marguerite River is a gravel bedded salmon river flowing in a valley carved by quaternary era glaciers. Bed material is composed of well mixed igneous and metamorphic rocks [*Dubé*, 1994]. The lithological composition of this mixture is stable along the channel length and thus no spatially dependent clast color variations can be observed. Suspended sediment load along the channel is not altered by tributaries and therefore the suspended sediment load can be assumed as constant for the whole channel. Channel width in the Sainte-Marguerite River varies from a few meters at the headwaters to approximately 80 m at the mouth. Most of this river is easily accessible for fieldwork purposes thanks to a paved road that follows the valley floor.

[9] This study covered the full 80 km of the main branch. In August 2002, a helicopter survey was carried out during the summer period of low flow. The airborne surveys were conducted at an altitude of 155 m between 10 am and 3 pm. Weather conditions were generally cloudy and dry with sunny spells. The XEOS™ imaging system, developed by Génivar, Inc., was fitted to a helicopter in order to obtain plan view digital imagery of the entire study area. For the selected flying height of 155 m, this resulted in images with a ground resolution of 3 cm (1:350 scale). Image format was 3008 pixels × 1960 pixels in the standard visible bands of red, green and blue. Images were collected at 60% overlap to allow for photogrammetric work to be carried out in the future. Two days were required to complete the surveys yielding 4184 images. Figure 1a shows a gray scale example of the resulting imagery. Since the images have 60% overlap, full coverage of the 80 km study reach can still be achieved by using every other image. Therefore 2092 images were used in this study. Precise georegistration of the images was not available and it was not possible to set a sufficient number of georeferenced control points in the field because of the sheer number (>6000) that would have been necessary. However, for each image, the helicopter position was recorded with the onboard GPS system. Therefore the position of each image center point is known.

2.2. Validation Data

[10] An independent set of grain size data was collected in the field to provide validation for the automated grain size measurements in submerged areas. Georeferenced manual samples of the surface grain size within the wetted perimeter were conducted at 39 field sites. For each site, 10 clasts were randomly extracted from the river bed in a 1 m^2 area and manually measured along the b axis. Water depth was measured for each site. Spatially, the sampling sites were scattered over approximately 20 km. Therefore each site is located in a different image and 39 images were processed. Each of these images was manually georeferenced with ARCMAP GIS software in order to position the data sites on the image. The estimated error of this process was ±29.7 cm.

[11] The measurements of Davey and Lapointe (C. E. Davey and M. F. Lapointe, Geography Department, McGill University, Application of the sedimentary link concept on the Sainte-Marguerite River: Preliminary findings, unpublished report, 2004, hereinafter referred to as Davey and Lapointe, unpublished report, 2004) were used as additional validation data in relation to the overall system-scale variability in grain size. This study established a field-based characterization of the sedimentary links on the Sainte-Marguerite River. It operated by bulk sampling of river bed material and field observations along the river channel made possible by the access road. These allowed the authors to locate link transitions defined as transitions from sand or fine particles to boulder rapids. The extent of sedimentary links presented in this report is qualitatively compared with the automated long profile to determine if the sedimentary links can be identified with automated grain size mapping. Thus, rather than the detailed quantitative validation implied in the sampling of grain sizes, the Davey and Lapointe (unpublished report, 2004) data allow us to assess the extent to which the method we develop is sufficient for geomorphological investigation of the kind conventionally undertaken using field sampling.

2.3. Image Classification

[12] The automated image classification algorithm discussed by *Carbonneau et al.* [2004], capable of identifying dry areas in an image, was developed further to perform automated classifications that could distinguish between vegetated and wetted areas. This algorithm operates in the MATLAB environment, as do all the methods presented in this paper. First, built-in MATLAB functions are used to transform the RGB color image to hue-saturation-intensity (HSI) format. The transformation from RGB to HSI format is analogous to the transformation from Cartesian to polar coordinates [*Castleman*, 1996]. In the HSI format, the color of a pixel is represented by an Intensity which is a vector norm combined with Hue and Saturation values which are equivalent to orbital and azimuthal angles in polar coordinates. The automated image segmentation procedure works by automated histogram partitions in the Hue and Intensity

bands. Examination of the Hue band histograms for the image set revealed that three distinct modes were generally present. The first mode corresponds to a merging of dry exposed sediment and optically shallow wetted sediment. The second mode corresponds to the vegetated area and the third mode corresponds to the optically deep wetted areas. An automated histogram partition was performed with a mimima finding function based on numerical derivatives. This allowed for three initial classes to be established: merged dry and optically shallow water, vegetated and optically deep water. Then attention was focused on the intensity band. It was found that if vegetated and deep water areas are masked out, the remaining histogram has two modes, one for the dry area and one for shallow area. Therefore automated partitioning of these two modes allowed for the areas and shallow areas to be classified.

[13] The precision of this classification procedure was estimated by randomly taking 10 images and comparing the automated classification with a manual classification where image classes were delimited by hand. Image pixels were then labeled as 1 for a correct classification and 0 for a false classification. This resulted in approximately 80% of pixels being correctly classified. The results of this quality estimation were not encouraging and led to the conclusion that the automated classification outputs needed to be corrected. Since the implementation of advanced automated classification algorithms was not a priority for this research, it was decided to correct the image classifications manually. Therefore a semiautomated interface was designed in the MATLAB environment to allow for a rapid and efficient editing process. This interface was designed to manage repetitive tasks such as image uploading and saving while taking advantage of human pattern recognition skills to identify and correct classification errors. The interface displays both the image and the raw classification image. The user can then rapidly correct classification errors by drawing directly on the image. With this interface, a single user can edit approximately 200 image classifications per day.

2.4. Extension of Semivariance Mapping to Wet Areas

[14] Examination of Figure 1a shows that, in the wetted area, portions of the bed are visible through the water interface. This suggests that textural information is still present and that grain size estimations could still be carried out. Therefore the method established by *Carbonneau et al.* [2004] is applied to the shallow wetted areas in order to test this hypothesis. Before applying the method, two factors must be considered. First, is equation (1) valid for submerged grains? Second, is the local semivariance window size (33×33 pixels) used to obtain equation (1) appropriate for submerged grains? Since it can be expected that the addition of a water interface will dampen the semivariance signal, it is highly unlikely that equation (1) will remain valid for submerged grains. Therefore the relationship between local semivariance and median grain size will need to be recalibrated. With respect to the appropriate window size, the work presented by *Carbonneau et al.* [2004] concluded that successful calibration was dependent on several factors. First, the sampling window must be sufficiently large to get a stable semivariance signal. Second, the gravel patches under consideration must be uniform on a spatial scale similar to that of the sampling window and of the calibration data sampling area. Finally, the smallest detectable grain size should be greater than the image resolution. These factors are not affected by the addition of the water interface and it was decided to retain the 33×33 pixel window size for the purposes of recalibration.

[15] Given the quality of the results in the dry bed area, the estimated dry bed grain size mapping results were used to generate calibration points. In order to do this, it was assumed that the grain size on either side of the wet/dry interface was approximately equal if the gravel patches were visibly uniform. The test site used by *Carbonneau et al.* [2004] was once again selected. Therefore large visibly uniform patches straddling the wet dry interface, in the five images necessary to get complete coverage of the test site, were identified. The grain size estimation algorithm was then used to measure the grain size in the dry area of the uniform patches. Additionally, the semivariance mapping algorithm was used to produce a semivariance map of the wetted area in the uniform patches. An algorithm programmed to follow the wet/dry interface was then used to subdivide the uniform patches into control data. For each meter length of the wet/dry interface, the algorithm stored the grain size in the adjacent 1 m^2 dry area and the semivariance in the adjacent 1 m^2 wet area. In this manner, 216 calibration points, each with a surface of 1 m^2, were collected from five images.

2.5. Automated Grain Size Measurement Processing Chain

[16] Provided the calibration and validation of individual grain size maps gives satisfactory results in the wetted optically shallow area, all the images in the data set will need to be processed. As stated earlier, all the processing is done in the MATLAB environment. First, a built-in MATLAB function is used to transform the RGB image to 8-bit gray scale. Then the edited image classification is used to isolate the dry area and the shallow wetted area in the gray scale image. Each of these image classes is then copied into a new blank image with all other class pixels initially set to zero. This results in a first image with only the dry area, the dry class image, and a second image with only the shallow area, the shallow class image. Before proceeding to the semivariance mapping, the mean brightness value for each image class is calculated. Then, the zero value pixels for a given class image are set to the corresponding mean brightness value. This is done in order to minimize the edge contrast between the masked area and the class-imaged area. Semivariance mapping is then carried out on both images by applying a windowed local semivariogram equation as described by *Carbonneau et al.* [2004]. The semivariance maps are then converted to grain size maps. Equation (1) is used to convert the dry class image semivariogram map to grain sizes and the calibration relationship obtained for the shallow area, given further as equation (2) is used to convert the shallow class image to grain sizes.

2.6. Automated Long Profile Measurements

[17] The resulting grain size maps can then be used to extract grain sizes in a downstream direction. A profiling algorithm was developed in the MATLAB environment to automatically perform this task. First, the channel is approximated as being linear at the scale of a single image. Then the image classification algorithm is used to find the channel and its orientation in the image. Once the orienta-

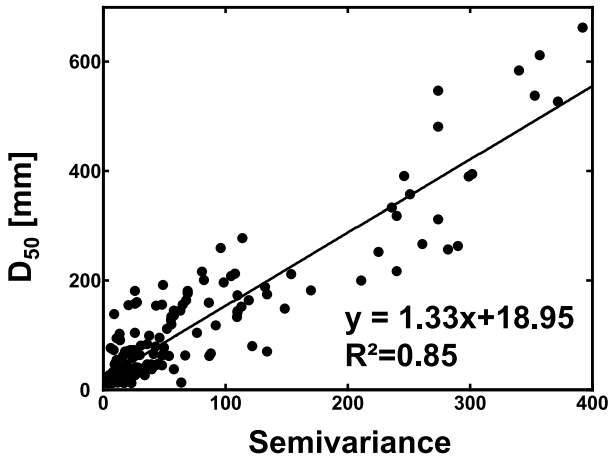

Figure 2. Calibration model for grain size estimation in submerged areas.

tion of the channel is known, a rotation algorithm is used to rotate the image in order to position the channel in a vertical orientation. This systematically places the channel in the same orientation as the pixel grid and thus simplifies the determination of the grain size sampling distances. The new rotated image is then divided into horizontal sampling area slices having a downstream length corresponding to the user specified sampling distance. Finally, the algorithm calculates the median grain size of all available automated grain size measurements within each sampling slice. This entire process is fully automated and can therefore be repeated for all the grain size maps.

[18] The position along the channel of each grain size measurement was then established from the GPS coordinates of each image center. These geographic GPS coordinates were first converted into a 1D "km" river coordinate system giving the distance upstream, along the river path, from the river mouth to each image. Then this distance from the river mouth and the pixel size were used to calculate the km rating of each sampling area slice thus allowing the profiling algorithm to output grain size as a function of distance upstream.

2.7. Overall Feasibility, Costs, and Processing Times

[19] While centimeter-scale resolution imagery is required for this method, such imagery is not difficult to obtain with current airborne remote sensing technology. For the present study, image acquisition cost is evaluated at approximately 200 US$ per river kilometer at 2005 prices, including both image acquisition and helicopter time. However, researchers considering applying these methods should note that if only short reaches are to be imaged, initial mobilization costs will make this figure increase by as much as an order of magnitude. Similarly, image surveys of very wide river systems may incur higher costs because of the necessity of multiple parallel flight lines. In addition to the air surveys, the work described here required roughly 4–5 person weeks of field work to collect the necessary calibration and validation data. In the preprocessing phase, classification edition required roughly 0.2 person/days per river kilometer and the processing time for grain size map production is approximately 4 hours per river kilometer on a current desktop PC. Finally, long profile extraction requires approximately 20 min per river kilometer.

3. Results

[20] Figure 2 shows the results of the calibration modeling. It can be seen that the relationship between local semivariance and median grain size is highly significant. The equation giving the median diameter as a function of local semivariance of the wetted region is

$$D_{50} = 1.33\mathrm{SV} + 18.95, \tag{2}$$

where D_{50} is the median diameter of surface particles, in mm, in the 1 m^2 area and SV is the dimensionless local variance sill value in the corresponding 1 m^2 area of the image. As hypothesized, the steeper slope in (2) as compared with (1) reflects the dampening of the semivariance signal in wetted areas as compared with dry areas, resulting in a greater change of D_{50} for a smaller change in semivariance. The level of explanation in the relationship is 85% (Figure 2) and this is sufficient for it to be used to estimate grain size in the wetted perimeter. Figure 3 shows the wetted median grain size maps obtained from the application of equation (2) to the whole wetted area in Figure 1a.

[21] Equation (2) was then used to process the 39 validation site images. The grain size values predicted by the algorithm were then compared with the values observed in the field. Figure 4 shows the model validation results. Observed grain size is plotted versus predicted grain sizes. The mean of the error gives a bias of −8 mm and the standard deviation of the error yields a precision of ±29 mm.

[22] The full set of 2092 images was then processed in order to obtain grain size maps for the entire river. Depth measurements collected for a separate paper [*Carbonneau et al.*, 2005] have allowed us to establish that the riverbed is optically shallow at depths of approximately 150 cm. Automated grain size measurements therefore cover all depths from 0 cm (i.e., dry areas) to 150 cm. In total, the grain size maps calculated for both the shallow wetted and

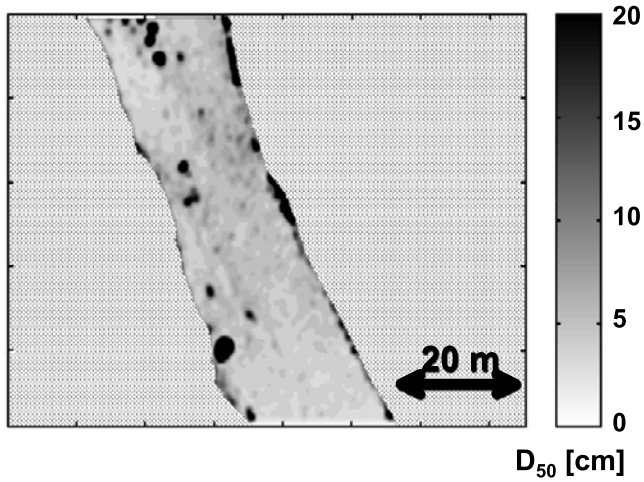

Figure 3. Median grain size map for the submerged areas of Figure 1a.

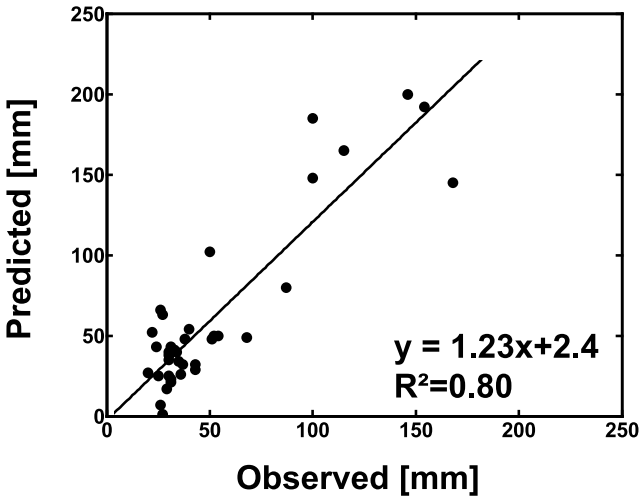

Figure 4. Validation results for the submerged grain size model.

dry areas of the whole river covered 86% (Table 1) of the active channel surface with 3.04 million, 1 m resolution, automated grain size measurements, evenly spaced in both downstream and cross-stream directions. The profiling algorithm was then applied to construct a long profile of median grain size with a regular 20 m sample spacing. Figure 5 shows the resulting long profile with vertical bars representing the link cutoff points as determined independently from field survey by Davey and Lapointe (unpublished report, 2004). The profile in Figure 5 has 4047 median grain size points. Among these, approximately 100 (≈2.5% of total) gross outliers can be observed. The correspondence between field-based link cutoff points and automatically measured grain size variations is very good. Unfortunately, short data gaps can be seen in the long profile in the vicinity of km points 18 and 80. These represent short periods of camera malfunctions where no image data are available.

4. Discussion

[23] When compared with *Carbonneau et al.* [2004] there is a degradation in the quality of the application of the method to subaqueous zones. There are three potential causes of this degradation: the effect of water depth on error, the effect of particle size on error, and the effect of substrate composition on error.

[24] The presence of a water interface will predictably degrade the quality of the automated grain size mapping results. Figure 6a shows a plot of the validation residuals (i.e., predicted D_{50} minus observed D_{50}) versus depth. The presence of nonlinear trend, with notably greater residual error at greater depths, suggests poorer grain size estimates in deeper parts of the flow. A depth-dependent calibration may be valuable for future applications, but this will require larger calibration data sets with a range of both depth and grain size information allowing for a grain size model which is a function of both local semivariance and local depth measurements.

[25] Closer examination of Figure 6a reveals that shallowest parts of the flow, with depths roughly below 50 cm, seem to have a systematic overestimation (negative error) of particle size while deeper parts of the flow have a systematic underestimation of particle size. Following this observation, accuracy and precision were re-estimated for flow depths below 50 cm and above 50 cm. For flow depths below 50 cm, accuracy and precision were estimated at −8 mm and ±13 mm, respectively. For flow depths above 50 cm, accuracy and precision were estimated at +10 mm and ±15 mm, respectively. Therefore the precision of wetted area grain size estimates in the first 50 cm of the flow is similar to that of the dry bed areas (±11 mm [*Carbonneau et al.*, 2004]).

[26] Closer examination of the grain size maps suggests that the median grain size of very coarse bed patches tends to be underestimated. Figure 6b shows a plot of the validation residuals vs. observed median diameter. A strong correlation between the error and the particle size is found up to values somewhere between 80 and 90 mm. This shows that the current median grain size estimation model becomes less reliable as bed material gets coarser, although the reliability does not continue to degrade for grain sizes greater than 90 mm. This effect can be explained by the relative areas of single particles and the semivariance mapping window. As bed material becomes coarser, the area of a single particle relative to the search window becomes more important. Thus fewer particles are contained

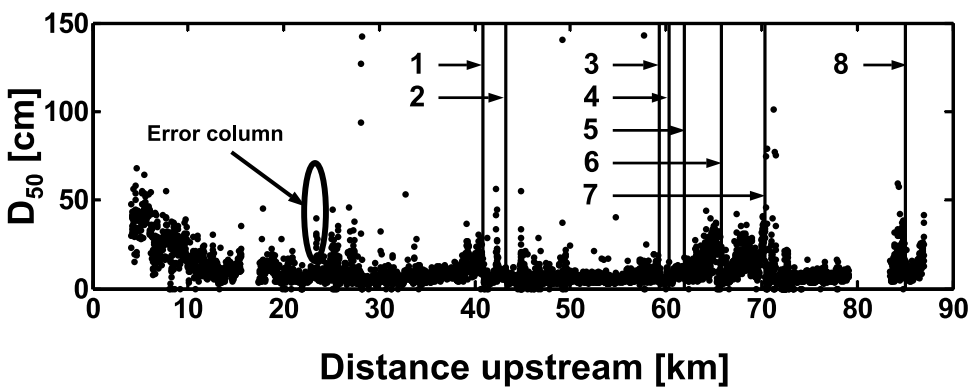

Figure 5. Long profile of median grain size showing link cutoff points (vertical lines), numbered 1–8 as determined by Davey and Lapointe (unpublished report, 2004) and an example of an "error column" structure caused by glare at the water surface.

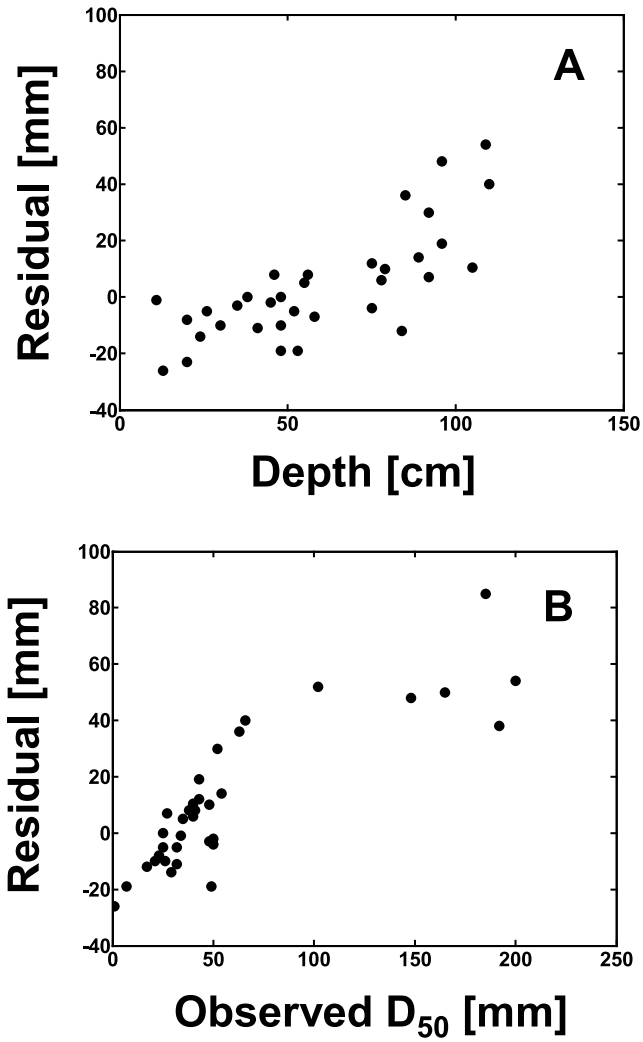

Figure 6. Structured residuals: (a) Scatterplot of validation residuals versus depth and (b) scatterplot of validation residuals versus size.

within the search window. Since contrast and semivariance levels are produced by the shaded area on the edge of particles, reducing the number of particles in the window likely reduces the semivariance and thus changes the calibration relationship. This suggests that the calibration relationship should not be linear. The apparent linear trend in the current calibration might be explained by an insufficient number of very coarse, boulder type, bed patches in the data set. Future applications of this method should therefore endeavor to have a higher number of coarse sized points in the calibration data set to allow for any nonlinear trend to become apparent.

[27] Variations in substrate composition could also account for some of the error of this method. *Legleiter et al.* [2004] have noted that different rock types have different radiative transfer properties and thus it would be reasonable to suggest that changes in rock type could alter local image properties. However, in the present case, the uniform lithological mix of the area makes this possibility less likely. An additional effect that can be included in substrate composition is the presence of algae growth such as periphyton. *Legleiter et al.* [2004] found that periphyton has different radiative transfer properties to those of gravels. Field observations clearly show that periphyton has a darker color than surrounding clean rocks and therefore it is likely that the presence of localized periphyton altered local contrasts and induced error.

[28] Comparison of the automated profile and field-based identification of link cutoff points (vertical bars in Figure 5) shows good agreement thus giving further validation to the method. Examination of the link cutoff bars shows that cutoffs 1, 3 7 and 8 have an excellent visual correspondence with automatically measured grain sizes. In the cases of link cutoff bars 2, 4, 5 and 6, field observations confirm that the grain size changes were subtler. Closer examinations of Figure 5 does show that smaller-scale grain size variations can be observed at link cutoff points 2, 4, 5 and 6. Furthermore, Figure 5 shows multiple structures not associated with known sedimentary links. It must therefore be determined if these structures are of natural origin or associated with measurement errors. At the downstream end of the profile, from 0 to 18 km, an important structure of *upstream* fining can be seen in Figure 5. Field investigations in this area have confirmed the existence of this structure and established that the river gradually cuts into a glacial till with very coarse particles. Therefore this upstream fining structure reflects a localized input of sediment, which is too coarse to be mobilized by the river. Another example of a valid structure not associated with sedimentary links can be seen in Figure 5 between link cutoffs 6 and 7. Here a cycle of coarsening and fining can be observed in the middle of the link. During the link identification work of Davey and Lapointe (unpublished report, 2004), this structure had not been found since it was in an area where access to the river was more difficult. Therefore it was initially thought that this feature in the automated profile was erroneous. However, subsequent field investigations found that this structure was real. As a consequence, the link definitions were updated and a new link cutoff point was added. This demonstrates that, in certain cases, remote sensing methods can be more accurate than the field sampling methods which are traditionally used to validate them. In particular, when field sites are inaccessible, remote sensing–based methods will bring important advantages in accuracy and cost effectiveness. Furthermore, the presence of smaller structures in the grain size profile of Figure 5 shows that automated grain size mapping could be used to investigate smaller-scale features. For example, continuous grain size mapping and the resulting long profile could be used to study the pool riffle sequence on a much larger scale and with a much improved sampling resolution than has been previously possible.

[29] While field observations have established that valid small-scale structures can be measured with automated grain size mapping, certain features in Figure 5 are associated with errors and the examination of the long profile in Figure 5 shows that a relatively small number of outliers (i.e., $\approx$100 points out of 4047) are present. These outliers were investigated by examining the source image and corresponding grain size map. This examination revealed that glary reflections on the water surface are an important source of error in the process. First, a uniform glare on the surface masks the river bed and replaces it with a low-

contrast area which is falsely interpreted as fine material. Second, in wave-generating windy conditions, glary reflections occur on wave crests only, leaving the troughs of the waves dark. This leads to a highly textured light-dark pattern on the water surface which is falsely interpreted as coarse submerged clasts and causes an important overestimation of grain sizes. These overestimations of grain size tend to be tightly clustered into groups and can be seen in Figure 5 as ''error columns.'' Figure 5 shows an example of such structures. Removal of these structures is difficult to automate and best carried out manually. Careful examination of the source imagery shows that the glare effect is not a binary phenomena which is either fully present or fully absent, glare intensity is a continuum and glare was found to be present in large areas at weak levels. This makes the establishment of a threshold for automated glare detection difficult and justifies the use of manual removal. In addition to a manual removal of glary points during postprocessing, steps to alleviate glare related errors can be implemented during data collection. A polarizing filter can be added to the camera lens to eliminate reflections from the water surface. This should minimize the presence of glary reflections and reduce the work needed in the postprocessing phase.

5. Conclusion

[30] It has been demonstrated that automated image processing methods can yield grain size information in coarse, optically shallow fluvial environments. Furthermore, the examination of the validation residuals has yielded additional insights into the workings of this grain size measurement method that could potentially lead to improved performance in future applications. Additionally, this paper has shown that such methods could be applied on a larger scale to study grain size variations along the entire channel length. The methods presented here therefore offer an unprecedented combination of meter-scale sampling resolution continuously applied to kilometer-scale areas.

[31] **Acknowledgments.** This work was a part of the Geosalar project, which is funded by the GEOIDE network of centers of excellence and our private sector partners Hydro-Québec and Génivar, Inc. This work received additional funding from the NATEQ postdoctoral scholarship program and is a contribution to the program of the Centre Interuniversitaire de Recherche sur le Saumon Atlantique (CIRSA).

References

Adams, J. (1979), Gravel size analysis from photographs, *J. Hydrol. Div. Am. Soc. Civil Eng.*, *105*(10), 1247–1255.

Bluck, B. J. (1982), The texture of gravel bars in braided streams, in *Gravel Bed Rivers*, edited by R. D. Hey, C. R. Thorne, and J. C. Bathurst, pp. 339–355, John Wiley, Hoboken, N. J.

Butler, J. B., S. N. Lane, and J. H. Chandler (2001), Automated extraction of grain-size data from gravel surfaces using digital image processing, *J. Hydraul. Res.*, *39*(5), 1–11.

Carbonneau, P. E., S. N. Lane, and N. E. Bergeron (2004), Catchment-scale mapping of surface grain size in gravel bed rivers using airborne digital imagery, *Water Resour. Res.*, *40*, W07202, doi:10.1029/2003WR002759.

Carbonneau, P. E., S. N. Lane, and N. E. Bergeron (2005), Feature based image processing methods applied to bathymetric measurements from airborne remote sensing in fluvial environments, *Earth Surf. Processes Landforms*, in press.

Castleman, K. R. (1996), *Digital Image Processing*, 666 pp., Prentice-Hall, Upper Saddle River, N. J.

Cunjak, R. A. (1988), Behaviour and microhabitat of young Atlantic salmon (*salmo salar*) during winter, *Can. J. Fish. Aquat. Sci.*, *45*, 2156–2160.

Cunjak, R. J. (1996), Winter habitat of selected stream fishes and potential impacts from land-use activities, *Can. J. Fish. Aquat. Sci.*, *53*, suppl. 1, 267–282.

Dubé, C. (1994), *Géologie du Québec*, 154 pp., Publ. du Québec, Quebec, Que., Canada.

Dunham, J. B., and B. E. Rieman (1999), Metapopulation structure of bull trout: Influences of physical, biotic, and geometrical landscape characteristics, *Ecol. Appl.*, *9*, 642–655.

Fausch, C. D., C. E. Torgersen, C. V. Baxter, and H. W. Li (2002), Landscapes to riverscapes: Bridging the gap between research and conservation of stream fishes, *Bioscience*, *52*, 483–498.

Folt, C. L., K. H. Nislow, and M. Power (1998), Implications of temporal and spatial scale for Atlantic salmon (*Salmo salar*) research, *Can. J. Fish. Aquat. Sci.*, *55*, suppl. 1, 9–21.

Ghalib, A. M., and R. D. Hryciw (1999), Soil particle size distribution by mosaic imaging and watershed analysis, *J. Comput. Civil Eng.*, *13*(2), 80–87.

Heggenes, J. (1996), Habitat selection by brown trout (*salmo trutta*) and young Atlantic salmon (*s. salar*) in streams: Static and dynamic hydraulic modelling, *Reg. Rivers Res. Manage.*, *12*, 155–169.

Hoey, T. B., and R. I. Ferguson (1994), Numerical simulation of downstream fining by selective transport in gravel bed rivers: Model development and illustration, *Water Resour. Res.*, *30*, 2251–2260.

Ibbeken, H., and R. Schleyer (1986), Photo sieving: A method for grainsize analysis of coarse-grained, unconsolidated bedding surfaces, *Earth Surf. Processes Landforms*, *11*, 59–77.

Legleiter, C. J., D. A. Roberts, W. A. Marcus, and M. A. Fonstad (2004), Passive remote sensing of river channel morphology and in-stream habitat: Physical basis and feasibility, *Remote Sens. Environ.*, *93*, 493–510.

Lewis, C. A., N. P. Lester, A. D. Bradshaw, J. E. Fitzgibbon, K. Fueller, L. Hakanson, and C. Richards (1996), Considerations of scale in habitat conservation and restoration, *Can. J. Fish. Aquat. Sci.*, *53*, suppl. 1, 440–445.

Lyon, J. G., R. S. Lunetta, and D. C. Williams (1992), Airborne multispectral scanner data for evaluating bottom sediment types and water depths of the St. Mary's River, Michigan, *Photogramm. Eng. Remote Sens.*, *58*, 951–956.

Marcus, W. A. (2002), Mapping of stream microhabitats with high spatial resolution hyperspectral imagery, *J. Geogr. Syst.*, *4*, 113–126.

Marcus, W. A., C. J. Leigleiter, R. J. Aspinall, J. W. Boardman, and R. L. Crabtree (2003), High spatial resolution hyperspectral mapping of in-stream habitats, depths, and woody debris in mountain streams, *Geomorphology*, *55*, 363–380.

Milne, J. A. (1982), Bed material size and the riffle pool sequence, *Sedimentology*, *29*, 267–278.

Parker, G. (1991), Selective sorting and abrasion of river gravel: 1. Theory, *J. Hydraul. Eng.*, *117*, 131–149.

Raschke, S. A., and R. D. Hryciw (1997), Grain-size distribution of granular soils by computer vision, *Geotech. Test. J.*, *20*(4), 433–442.

Rice, S. P. (1999), The nature and controls on downstream fining within sedimentary links, *J. Sediment. Res.*, *69*, 32–39.

Rice, S. P., and M. Church (1996), Bed material texture in low order streams on the Queen Charlotte Islands, British Columbia, *Earth Surf. Processes Landforms*, *21*, 1–18.

Rice, S. P., and M. Church (1998), Grain size along two gravel-bed rivers: Statistical variations, spatial patterns and sedimentary links, *Earth Surf. Processes Landforms*, *23*, 345–363.

Rice, S. P., M. T. Greenwood, and C. B. Joyce (2001a), Tributaries, sediment sources, and the longitudinal organisation of macroinvertebrate fauna along river systems, *Can. J. Fish. Aquat. Sci.*, *58*, 824–840.

Rice, S. P., M. T. Greenwood, and C. B. Joyce (2001b), Macroinvertebrate community changes at coarse sediment recruitment points along two gravel bed rivers, *Water Resour. Res.*, *37*, 2793–2803.

Rimmer, D. M., U. Paim, and R. L. Saunders (1983), Changes in the selection of microhabitat by juvenile Atlantic salmon (*salmo salar*) at the summer-autumn transition in a small river, *Can. J. Fish. Aquat. Sci.*, *41*, 469–475.

Roberts, A. C. B., and J. M. Anderson (1999), Shallow water bathymetry using integrated airborne multi-spectral remote sensing, *Int. J. Remote Sens.*, *20*, 497–510.

Seal, R., and C. Paola (1995), Observations of downstream fining on the North Fork Toutle River near Mount St. Helens, Washington, *Water Resour. Res.*, *31*, 1409–1419.

Seal, R., C. Paola, G. Parker, J. B. Southard, and P. R. Wilcock (1997), Experiments on downstream fining of gravel: 1. Narrow channel runs, *J. Hydraul. Eng.*, *123*, 874–884.

Shin, S., and R. D. Hryciw (2004), Wavelet analysis of soil mass images for particle size determination, *J. Comput. Civil Eng.*, *18*(1), 19–27.

Thompson, W. L., and D. C. Lee (2000), Modeling relationships between landscape-level attributes and snorkel counts of chinook salmon and steelhead parr in Idaho, *Can. J. Fish. Aquat. Sci.*, *57*, 1834–1842.

Torgersen, C. E., D. M. Price, H. W. Li, and B. A. McIntosh (1999), Multiscale thermal refugia and stream habitat associations of chinook salmon in northeastern Oregon, *Ecol. Appl.*, *9*, 301–319.

Westaway, R. M., S. N. Lane, and D. M. Hicks (2003), Remote survey of large-scale braided rivers using digital photogrammetry and image analysis, *Int. J. Remote Sens.*, *24*, 795–816.

Whited, D., J. A. Stanford, and J. S. Kimball (2002), Application of airborne multispectral digital imagery to quantify riverine habitats at different base flows, *River Res. Appl.*, *18*, 583–594.

Wettimuny, R., and D. Penumadu (2004), Application of Fourier analysis to digital imaging for particle shape analysis, *J. Comput. Civil Eng.*, *18*(1), 2–9.

Winterbottom, S. J., and D. J. Gilvear (1997), Quantification of channel bed morphology in gravel-bed rivers using airborne multispectral imagery and aerial photography, *Reg. Rivers Res. Manage.*, *13*, 489–499.

N. Bergeron, Centre Eau, Terre et Environnement, INRS, 490 Rue de la Couronne, Québec, QC, Canada G1K 9A9.

P. E. Carbonneau and S. N. Lane, Department of Geography, University of Durham, Science Site, South Road, Durham DH1 3LE, UK. (patrice.carbonneau@dur.ac.uk)